

1 On the progress of the 2015–2016 El Niño event

2
3 **Costas A. Varotsos¹, Chris G. Tzanis¹ and Nicholas V. Sarlis²**

4 [1]{Climate Research Group, Division of Environmental Physics and Meteorology, Faculty of
5 Physics, University of Athens, University Campus Bldg. Phys. V, Athens, 157 84, Greece}

6 [2]{Department of Solid State Physics, Faculty of Physics, School of Science, National and
7 Kapodistrian University of Athens, Panepistimiopolis Zografos, 157 84 Athens, Greece}

8 Correspondence to: C. A. Varotsos (covar@phys.uoa.gr)

9 10 **Abstract**

11 It has been recently reported that the current 2015–2016 El Niño could become “one of the
12 strongest on record”. To further explore this claim, we performed the new analysis described
13 in detail in Varotsos et al. (2015) that allows the detection of precursory signals of the strong
14 El Niño events by using a recently developed non-linear dynamics tool. In this context, the
15 analysis of the Southern Oscillation Index time series for the period 1876–2015 shows that the
16 running 2015–2016 El Niño would be rather a “moderate to strong” or even a “strong” event
17 and not “one of the strongest on record”, as that of 1997–1998.

18 19 **1 Introduction**

20 El Niño/La Niña Southern Oscillation (ENSO) is an oceanic-atmospheric quasi-periodic
21 phenomenon with several impacts on climate and weather not only in the tropical Pacific, but
22 in many regions all over the world (Varotsos and Deligiorgi, 1991; Kondratyev and Varotsos,
23 1995a,b; Klein et al., 1999; Xue et al., 2000; Eccles and Tziperman, 2004; Cracknell and
24 Varotsos, 2007, 2011; Lin, 2007; Chattopadhyay and Chattopadhyay, 2011; Efstathiou et al.,
25 1998, 2011; Varotsos, 2013; Varotsos et al., 2009a, 2012, 2014a,b). The disastrous effects of
26 the strong ENSO events necessitate their reliable short and long-term prediction (Latif et al.,
27 1998; Stenseth et al., 2003; Monks et al., 2009; Hsiang et al., 2011; Cheng et al., 2011;
28 Barnston et al., 2012; Krapivin and Shutko, 2012; Tippett et al., 2012). In this context,
29 Varotsos et al. (2015) presented a new method (see also Varotsos and Tzanis, 2012) for the

1 detection of precursory signals of the strong El Niño events by using the entropy change in
2 “natural time” (a new time domain, see Varotsos et al., 2002) under time reversal. The
3 analysis of the Southern Oscillation Index (SOI) time series by using this modern method
4 provided significant precursory signals of two of the strongest El Niño events (1982–1983 and
5 1997–1998).

6 Very recently, Klein (2015) reported that the running 2015–2016 El Niño could become “one
7 of the strongest on record”. Furthermore, the Australian Government Bureau of Meteorology
8 (BOM) in their report
9 (http://www.bom.gov.au/climate/enso/archive/ensowrap_20150901.pdf) of 1 September 2015
10 stated that “The 2015 El Niño is now the strongest El Niño since 1997–98” and moreover on
11 29 September 2015 they reported that most international climate models indicate current El
12 Niño (http://www.bom.gov.au/climate/enso/archive/ensowrap_20150929.pdf) “is likely to
13 peak towards the end of 2015” as also reported on 8 October 2015 by the Climate Prediction
14 Center, National Centers for Environmental Prediction, National Oceanic and Atmospheric
15 Administration (NOAA)/National Weather Service
16 (http://www.cpc.ncep.noaa.gov/products/analysis_monitoring/enso_disc_oct2015/ensodisc.pdf).

17 In this study, we further explore these claims, by applying to the SOI time series the recently
18 proposed analysis by Varotsos et al. (2015). The ability of accurate predictions of such severe
19 natural events, like El Niño, is of crucial importance especially nowadays, where the global
20 annual average temperature in 2015 reached the warmest on record values, which might be
21 associated with the 2015 El Niño event (WMO, 2016).

22

23 **2 Results and discussion**

24 As mentioned in the previous section, we analyse the SOI time series (Troup, 1965; Power
25 and Kociuba, 2011) for the period January 1876 – October 2015 by employing the method
26 described in detail in Varotsos et al. (2015). More specifically, we conduct the analysis of the
27 SOI monthly values by using the dataset, entitled “Monthly SOI Phase 1887 – 1989 Base”,
28 (<https://www.longpaddock.qld.gov.au/seasonalclimateoutlook/southernoscillationindex/soidatafiles/index.php>)
29 derived from the Long Paddock site. It should be clarified that we use the monthly values of
30 SOI, instead of the daily ones, as the latter introduce significant noise due to daily weather
31 patterns variability. It should be noted here that El Niño and La Niña episodes are associated
32 with negative and positive values of the SOI, respectively, and $SOI =$

1 $10 \times [PA(\text{Tahiti}) - PA(\text{Darwin})] / SDD$, where the Pressure Anomaly (PA) is the monthly mean
2 minus long-term mean (1887–1989 base period) and SDD is the standard deviation of the
3 difference (1887–1989 base period) of mean sea level pressure between Tahiti and Darwin.

4 The method suggested by Varotsos et al. (2015) is based on the entropy change in natural time
5 under time reversal ΔS_i (e.g., see Varotsos et al., 2005, 2007, 2009b; Sarlis et al., 2010, 2011)
6 calculated for a window size of i events (SOI monthly values). To this end, Varotsos et al.
7 (2015) converted the original SOI time series to a new one $Q_k = (\text{SOI}_k + \text{lmin}(\text{SOI}))$, where
8 $\text{min}(\text{SOI})$ is the minimum value of SOI during the whole study period, keeping the temporal
9 sequence of the events and not considering their time of occurrence. Hence, for each Q_k value
10 we calculate the ratio (χ_k) of the order of its occurrence (k) and the total number (i) of events
11 within the window, i.e. $\chi_k = k/i$. The latter quantity, which replaces the conventional time
12 (t), is natural time χ_k characterizing the k -th event (Varotsos et al., 2002). This way,
13 Varotsos et al. (2015) introduced a new series the members of which are the pairs (χ_k, Q_k)
14 where $Q_k > 0$. Thus, one can define the quantity $p_k = Q_k / \sum_{n=1}^i Q_n$ which can be considered
15 as a probability, since it is positive and satisfies the condition $\sum_{n=1}^i p_n = 1$ (Varotsos et al.,
16 2011). Under these assumptions, the average values of quantities, which are functions of
17 natural time χ , can be evaluated by $\langle f(\chi) \rangle = \sum_{n=1}^i f(\chi_n) p_n$ and the entropy in natural time
18 can be defined by $S = \langle \chi \ln \chi \rangle - \langle \chi \rangle \ln \langle \chi \rangle$ (Varotsos et al., 2005, 2011). The latter quantity
19 changes to a value S_- if, instead of the true sequence of events, one uses the time-reversed
20 process that is described by $p'_k = \hat{T} p_k = p_{i-k+1}$, where \hat{T} denotes the time reversal operator in
21 the window of i events. The quantity $\Delta S_i (= S - S_-)$ reveals the breaking of time-symmetry by
22 capturing the difference in the dynamics as the system evolves from present to future and
23 vice-versa. In short, it has been shown (e.g., see Varotsos et al., 2007, 2011) that positive
24 values of ΔS_i correspond to a decreasing time-series in natural time, and hence when ΔS_i
25 exceeds a certain threshold this reveals that SOI is approaching at small values indicating El
26 Niño (Varotsos et al., 2015). Varotsos et al. (2015) have also shown (see their Fig. 4) that the
27 most useful window size for this purpose is $i = 20$ events (months). In their prediction scheme,
28 the monthly SOI values for the past 20 months are used for the calculation of ΔS_{20} (see the red
29 crosses in Figs. 1 and 3) and compared with a threshold ΔS_{thres} , which can be determined on

1 the basis of Receiver Operating Characteristics (ROC, see Fawcett, 2006). ROC is a method
 2 for the visualization, evaluation, and selection of prediction schemes based on their
 3 performance, which is quantified by a plot of the hit rate vs. the false alarm rate obtained by
 4 the following procedure applied to the present case. When $\Delta S_{20} \geq \Delta S_{\text{thres}}$, one issues an alarm
 5 that the value of SOI for the next month will be smaller than or equal to T (see the black
 6 broken line in Fig. 2). If this turns out to be true, then we have a true positive prediction. If
 7 $\Delta S_{20} < \Delta S_{\text{thres}}$ and the next month's SOI is larger than T , then we have a true negative
 8 prediction. All other combinations lead to errors (which are inevitable in stochastic
 9 prediction), which can be either false positive or false negative predictions. Figure 2 depicts
 10 the ROC curve obtained, when using ΔS_{20} as a predictor for the SOI value of the next month
 11 with $T = -14$ (which is the upper limit of the yellow area in Figs. 1 and 3 discussed below).
 12 This is a diagram of the hit rate (or True Positive rate, i.e., the number of true positive
 13 predictions over all cases with $\text{SOI} \leq T = -14$) vs. the false alarm rate (or False Positive rate,
 14 i.e., the number of false positive predictions over all cases with $\text{SOI} > -14$) as we vary ΔS_{thres} .
 15 A method to estimate an appropriate value of ΔS_{thres} is that of iso-performance lines suggested
 16 by Provost and Fawcett (1998, 2001). In this scheme, a line of constant slope m (see the blue
 17 line in Fig. 2) is selected on the basis of the relative cost of false positive predictions over the
 18 cost of false negative predictions multiplied by the relative frequency of negatives over
 19 positives, i.e., see Eq. (1) of Fawcett (2006). As a typical selection we chose $m = 1$. We fitted
 20 ROC points with the red curve (having a simple analytical form $a + b\sqrt{x} + cx^d$) and
 21 determined the point at which the slope was unity. This leads to the ROC point indicated by
 22 an arrow in Fig. 2 and corresponds to $\Delta S_{\text{thres}} = 0.0035$ (i.e., a value very close to that 0.00326
 23 presented in Table 1 of Varotsos et al (2015) for $T = -15$). Thus, in Figs. 1 and 3 when $\Delta S_{20} \geq$
 24 0.0035 the alarm is set on for the SOI value of the next month.

25 The time progress of the SOI monthly values as well as the entropy change in natural time
 26 under time reversal (for the window length $i = 20$ months) ΔS_{20} are depicted in Fig. 1 (as well
 27 as in Fig. 3). Beyond the information gained from the exploration of the ΔS_{20} dynamics and in
 28 order to further identify if 2015–2016 El Niño could be characterized as a “very strong” one
 29 or even more as “one of the strongest on record”, we followed the classification and
 30 characterization of the past El Niño events given by BOM
 31 (<http://www.bom.gov.au/climate/enso/enlist/>). The coloured areas in Figs. 1 and 3 represent
 32 the mean minimum negative values of SOI along with the 1σ standard deviation bands for the

1 two cases of “weak, weak to moderate, moderate, moderate to strong” (green band) and
2 “strong, very strong” (yellow band) El Niño events.

3 As can be clearly seen in Fig. 3, the SOI values during the last three months remain in the
4 green band and in the limits of the yellow one, indicating that 2015 El Niño should be rather
5 characterized as a “moderate to strong” or even “strong” event and not “one of the strongest
6 on record”, as also shown by comparing with the El Niño events of 1982–1983 and 1997–
7 1998. Furthermore, the variation of ΔS_{20} during the 2015 El Niño in comparison with 1982–
8 1983 and 1997–1998 El Niño events is not as sharp, confirming that the undergoing El Niño
9 event is not “one of the strongest on record”. In order to estimate the extent of this variation,
10 we plot with the black curve in Fig. 4 the probability density function (PDF) of ΔS_{20} obtained

11 from the estimator $f_N(\Delta S_{20}) = \frac{1}{N} \sum_{i=1}^N \frac{1}{b_N} K\left(\frac{\Delta S_{20} - O_i}{b_N}\right)$, where O_i are the observed values of

12 ΔS_{20} since the beginning of our study, N is the total number of these observations, the kernel
13 $K(x)$ is non-zero only when $|x| < 1$ having the value $K(x) = \frac{3}{4}(1-x^2)$ and b_N is related with the

14 standard deviation σ of the observed ΔS_{20} values by $b_N = 10.25\sigma/N^{0.34}$ as suggested by
15 Mercik et al. (1999). We observe in Fig. 4 that only rarely ΔS_{20} exceeds the value of 0.02,
16 which can be also verified by the red histogram obtained for ΔS_{20} using the TISEAN package
17 (Hegger et al., 1999) (also plotted in Fig. 4). In the latter histogram, the minimum non-zero
18 height is observed in the bar that includes the value $\Delta S_{20} = 0.02$ covering the range up to
19 approximately 0.0205. To detect when ΔS_{20} exceeds the latter value, we plot with blue crosses
20 the time series of ΔS_{20} vs. time, which can be read in the right axis of Fig. 4. We see (blue
21 arrows in Fig. 4) that $\Delta S_{20} > 0.0205$ is observed only in the three strong El Niño events of
22 1905-1906, 1982-1983 and 1997-1998. This inequality, however, is not fulfilled in the current
23 case (2015–2016 El Niño), since the currently observed values are close to 0.01, i.e.,
24 markedly smaller than the value of 0.0205.

25

26 **3 Conclusions**

27 Recent reports indicate that 2015–2016 El Niño event could become “one of the strongest on
28 record” or could be already characterized as “the strongest El Niño since 1997–98”. In order
29 to investigate these assertions, we analyzed the SOI time series for the period January 1876 –

1 October 2015 by using the method described in Varotsos et al. (2015) based on the entropy
2 change in natural time under time reversal. The results obtained indicate that the undergoing
3 2015–2016 El Niño event should be rather characterized as a “moderate to strong” or even
4 “strong” event and not “one of the strongest on record”.

5 **References**

6 Barnston, A. G., Tippett, M. K., L’Heureux, M. L., Li, S. H., and DeWitt, D. G.: Skill of real-
7 time seasonal ENSO model predictions during 2002–11: is our capability increasing? B.
8 Am. Meteorol. Soc., 93, 631–651, 2012.

9 Chattopadhyay, S. and Chattopadhyay, G.: The possible association between summer
10 monsoon rainfall in India and sunspot numbers, *Int. J. Remote Sens.*, 32, 891–907, 2011.

11 Cheng, Y. J., Tang, Y. M., and Chen, D. K.: Relationship between predictability and forecast
12 skill of ENSO on various time scales, *J. Geophys. Res.*, 116, C12006,
13 doi:10.1029/2011JC007249, 2011.

14 Cracknell, A. P. and Varotsos, C. A.: The Antarctic 2006 ozone hole, *Int. J. Remote Sens.*, 28,
15 1–2, 2007.

16 Cracknell, A. P. and Varotsos, C. A.: New aspects of global climate-dynamics research and
17 remote sensing, *Int. J. Remote Sens.*, 32, 579–600, 2011.

18 Eccles, F. and Tziperman, E.: Nonlinear effects on ENSO’s period, *J. Atmos. Sci.*, 61, 474–
19 482, 2004.

20 Efstathiou, M., Varotsos, C., and Kondratyev, K. Y.: An estimation of the surface solar
21 ultraviolet irradiance during an extreme total ozone minimum, *Meteorol. Atmos. Phys.*, 68,
22 171–176, 1998.

23 Efstathiou, M. N., Tzani, C., Cracknell, A. P., and Varotsos, C. A.: New features of land and
24 sea surface temperature anomalies, *Int. J. Remote Sens.*, 32, 3231–3238, 2011.

25 Fawcett, T.: An introduction to ROC analysis, *Pattern Recogn. Lett.*, 27, 861–874, 2006.

26 Hegger, R., Kantz, H. and Schreiber, T.: Practical implementation of nonlinear time series
27 methods: The TISEAN package, *Chaos*, 9, 413–435, 1999.

28 Hsiang, S. M., Meng, K. C., and Cane, M. A.: Civil conflicts are associated with the global
29 climate, *Nature*, 476, 438–441, 2011.

- 1 Klein, K.: NOAA predicts strong El Niño, *Eos*, 96, doi:10.1029/2015EO035535, 2015.
- 2 Klein, S. A., Soden, B. J., and Lau, N. C.: Remote sea surface temperature variations during
3 ENSO: Evidence for a tropical atmospheric bridge, *J. Climate*, 12, 917–932, 1999.
- 4 Kondratyev, K. Y. and Varotsos, C.: Atmospheric greenhouse effect in the context of global
5 climate change, *Il Nuovo Cimento C*, 18, 123–151, 1995a.
- 6 Kondratyev, K. Y. and Varotsos, C. A.: Volcanic-eruptions and global ozone dynamics, *Int. J.*
7 *Remote Sens.*, 16, 1887–1895, 1995b.
- 8 Krapivin, V. F. and Shutko, A. M.: Information technologies for remote monitoring of the
9 environment, Springer/Praxis, Chichester, UK, 2012.
- 10 Latif, M., Anderson, D., Barnett, T., Cane, M., Kleeman, R., Leetmaa, A., O’Brien, J., Rosati,
11 A., and Schneider, E.: A review of the predictability and prediction of ENSO, *J. Geophys.*
12 *Res.*, 103, 14375–14393, 1998.
- 13 Lin, J.-L.: Interdecadal variability of ENSO in 21 IPCC AR4 coupled GCMs, *Geophys. Res.*
14 *Lett.*, 34, L12702, doi:10.1029/2006GL028937, 2007.
- 15 Mercik, S., Weron, K., and Siwy, Z.: Statistical analysis of ionic current fluctuations in
16 membrane channels, *Phys. Rev. E*, 60, 7343–7348, 1999.
- 17 Monks, P. S., Granier, C., Fuzzi, S., Stohl, A., Williams, M. L., Akimoto, H., Amann, M.,
18 Baklanov, A., Baltensperger, U., Bey, I., Blake, N., Blake, R. S., Carslaw, K., Cooper, O.
19 R., Dentener, F., Fowler, D., Fragkou, E., Frost, G. J., Generoso, S., Ginoux, P., Grewe, V.,
20 Guenther, A., Hansson, H. C., Henne, S., Hjorth, J., Hofzumahaus, A., Huntrieser, H.,
21 Isaksen, I. S. A., Jenkin, M. E., Kaiser, J., Kanakidou, M., Klimont, Z., Kulmala, M., Laj,
22 P., Lawrence, M. G., Lee, J. D., Liousse, C., Maione, M., McFiggans, G., Metzger, A.,
23 Mieville, A., Moussiopoulos, N., Orlando, J. J., O’Dowd, C. D., Palmer, P. I., Parrish, D.
24 D., Petzold, A., Platt, U., Pöschl, U., Prévôt, A. S. H., Reeves, C. E., Reimann, S., Rudich,
25 Y., Sellegri, K., Steinbrecher, R., Simpson, D., ten Brink, H., Theloke, J., van der Werf, G.
26 R., Vautard, R., Vestreng, V., Vlachokostas, Ch., and von Glasow, R.: Atmospheric
27 composition change – global and regional air quality, *Atmos. Environ.*, 43, 5268–5350,
28 2009.
- 29 Power, S. B. and Kociuba, G.: The impact of global warming on the Southern Oscillation
30 Index, *Clim. Dynam.*, 37, 1745–1754, 2011.

- 1 Provost, F. and Fawcett, T.: Robust classification systems for imprecise environments, in:
2 Proceedings of the AAAI-98, Menlo Park, CA, 706–713, 1998.
- 3 Provost, F. and Fawcett, T.: Robust classification for imprecise environments, *Mach. Learn.*,
4 42, 203–231, 2001.
- 5 Sarlis, N. V., Skordas, E. S., and Varotsos, P. A.: Nonextensivity and natural time: The case
6 of seismicity, *Phys. Rev. E*, 82, 021110, doi:10.1103/PhysRevE.82.021110, 2010.
- 7 Sarlis, N. V., Skordas, E. S., and Varotsos, P. A.: The change of the entropy in natural time
8 under time-reversal in the Olami–Feder–Christensen earthquake model, *Tectonophysics*,
9 513, 49–53, 2011.
- 10 Stenseth, N. C., Ottersen, G., Hurrell, J. W., Mysterud, A., Lima, M., Chan, K. S., Yoccoz, N.
11 G., and Adlandsvik, B.: Studying climate effects on ecology through the use of climate
12 indices: the North Atlantic Oscillation, El Niño Southern Oscillation and beyond, *P. Roy.
13 Soc. Lond. B Bio.*, 270, 2087–2096, 2003.
- 14 Tippet, M. K., Barnston, A. G., and Li, S. H.: Performance of recent multimodel ENSO
15 forecasts, *J. Appl. Meteorol. Clim.*, 51, 637–654, 2012.
- 16 Troup, A. J.: The Southern Oscillation, *Q. J. Roy. Meteor. Soc.*, 91, 490–506, 1965.
- 17 Varotsos, C. A.: The global signature of the ENSO and SST-like fields, *Theor. Appl.
18 Climatol.*, 113, 197–204, 2013.
- 19 Varotsos, C. A. and Deligiorgi, D. G.: Sea-surface temperature and southern oscillation signal
20 in the upper stratosphere-lower mesosphere, *Int. J. Climatol.*, 11, 77–83, 1991.
- 21 Varotsos, C. A. and Tzani, C.: A new tool for the study of the ozone hole dynamics over
22 Antarctica, *Atmos. Environ.*, 47, 428–434, 2012.
- 23 Varotsos, C., Efstathiou, M., and Tzani, C.: Scaling behaviour of the global tropopause,
24 *Atmos. Chem. Phys.*, 9, 677–683, 2009a.
- 25 Varotsos, C. A., Cracknell, A. P., and Tzani, C.: The exceptional ozone depletion over the
26 Arctic in January–March 2011, *Remote Sens. Lett.*, 3, 343–352, 2012.
- 27 Varotsos, C., Christodoulakis, J., Tzani, C., and Cracknell, A. P.: Signature of tropospheric
28 ozone and nitrogen dioxide from space: A case study for Athens, Greece, *Atmos. Environ.*,
29 89, 721–730, 2014a.

- 1 Varotsos, C. A., Franzke, C. L. E., Efstathiou, M. N., and Degermendzhi, A. G.: Evidence for
2 two abrupt warming events of SST in the last century, *Theor. Appl. Climatol.*, 116, 51–60,
3 2014b.
- 4 Varotsos, C. A., Tzanis, C., and Cracknell, A. P.: Precursory signals of the major El Niño
5 Southern Oscillation events, *Theor. Appl. Climatol.*, doi:10.1007/s00704-015-1464-4,
6 online first, 2015.
- 7 Varotsos, P. A., Sarlis, N. V., and Skordas, E. S.: Long-range correlations in the electric
8 signals that precede rupture, *Phys. Rev. E*, 66, 011902, doi:10.1103/PhysRevE.66.011902,
9 2002.
- 10 Varotsos, P. A., Sarlis, N. V., and Skordas, E. S.: Detrended fluctuation analysis of the
11 magnetic and electric field variations that precede rupture, *Chaos*, 19, 023114,
12 doi:10.1063/1.3130931, 2009b.
- 13 Varotsos, P. A., Sarlis, N. V., Tanaka, H. K., and Skordas, E. S.: Some properties of the
14 entropy in the natural time, *Phys. Rev. E*, 71, 032102, doi:10.1103/PhysRevE.71.032102,
15 2005.
- 16 Varotsos, P. A., Sarlis, N. V., Skordas, E. S., and Lazaridou, M. S.: Identifying sudden cardiac
17 death risk and specifying its occurrence time by analyzing electrocardiograms in natural
18 time, *Appl. Phys. Lett.*, 91, 064106, doi:10.1063/1.2768928, 2007.
- 19 Varotsos, P. A., Sarlis, N. V., and Skordas, E. S.: *Natural Time Analysis: The new view of*
20 *time. Precursory Seismic Electric Signals, Earthquakes and other Complex Time-Series,*
21 Springer-Verlag, Berlin Heidelberg, 2011.
- 22 WMO (World Meteorological Organization), Press Release No. 2, 2016, available at:
23 <https://www.wmo.int/media/content/2015-hottest-year-record>.
- 24 Xue, Y., Llewellyn-Jones, D.T., Lawrence, S. P., and Mutlow, C. T.: On the Earth's surface
25 energy exchange determination from ERS satellite ATSR data: Part 3. Turbulent heat flux
26 on open sea, *Int. J. Remote Sens.*, 21, 3427–3444, 2000.

Figure captions

1

2

3 **Figure 1.** The entropy change ΔS_{20} in natural time for the window length $i = 20$ months (red
4 line, left scale) along with SOI monthly values (blue line, right scale) for the period January
5 1980 – October 2015. The alarm is set on (black line), when ΔS_{20} exceeds the threshold value
6 $\Delta S_{\text{thres}} = 0.0035$.

7

8 **Figure 2.** The hit rate vs. false alarm rate when using ΔS_{20} as a predictor for the SOI value of
9 the next month. The ROC point indicated by the arrow has been selected so that the slope of
10 the tangent of the analytical fitting of the ROC points indicated by the red curve has unit slope
11 and hence it corresponds to the $m = 1$ iso-performance line of the ROC space (e.g., see
12 Fawcett, 2006; Provost and Fawcett, 1998, 2001).

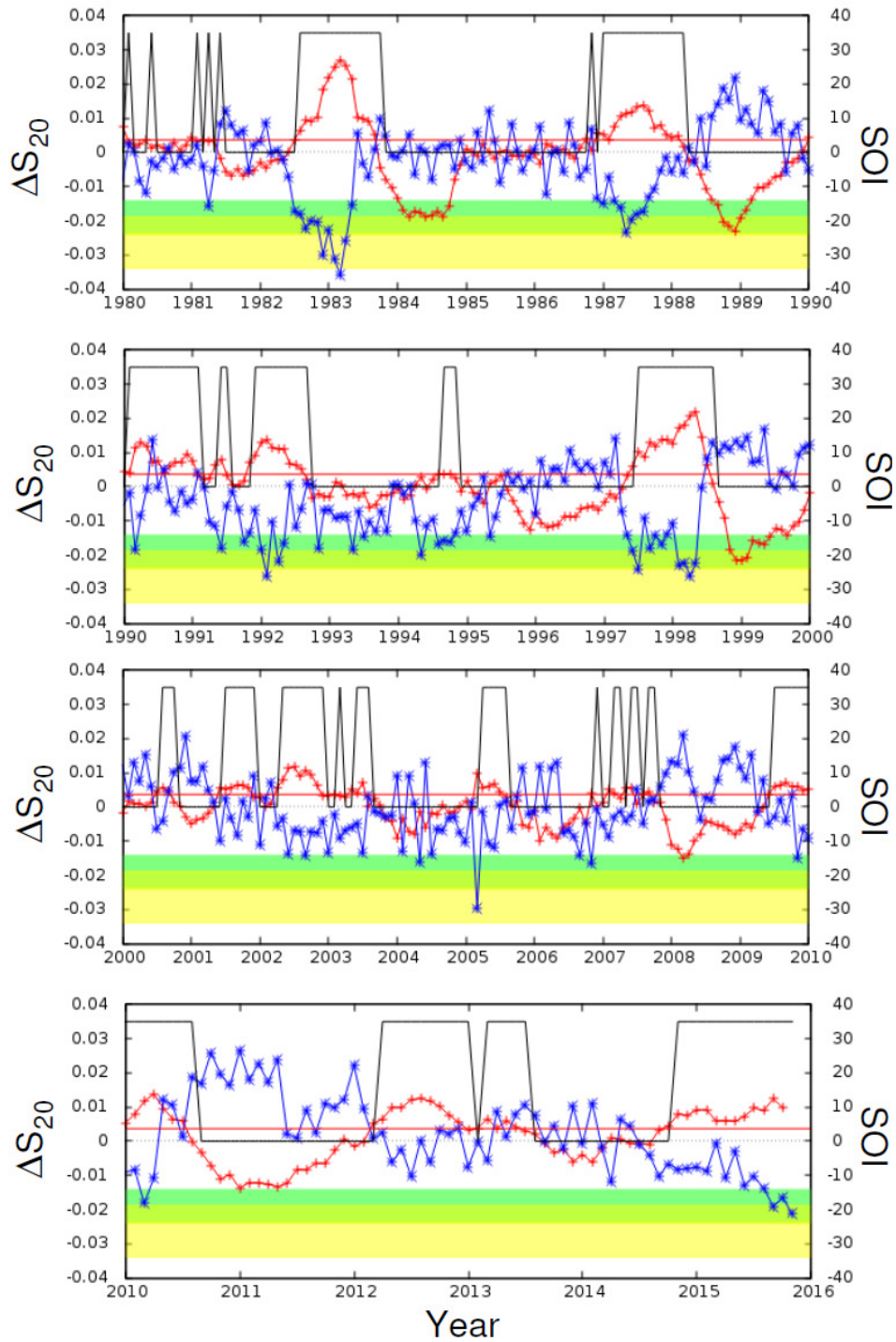
13

14 **Figure 3.** As in Fig. 1, but only for the 1982–1983, 1997–1998 (the two strongest in the last
15 century) and the current 2015–2016 El Niño events.

16

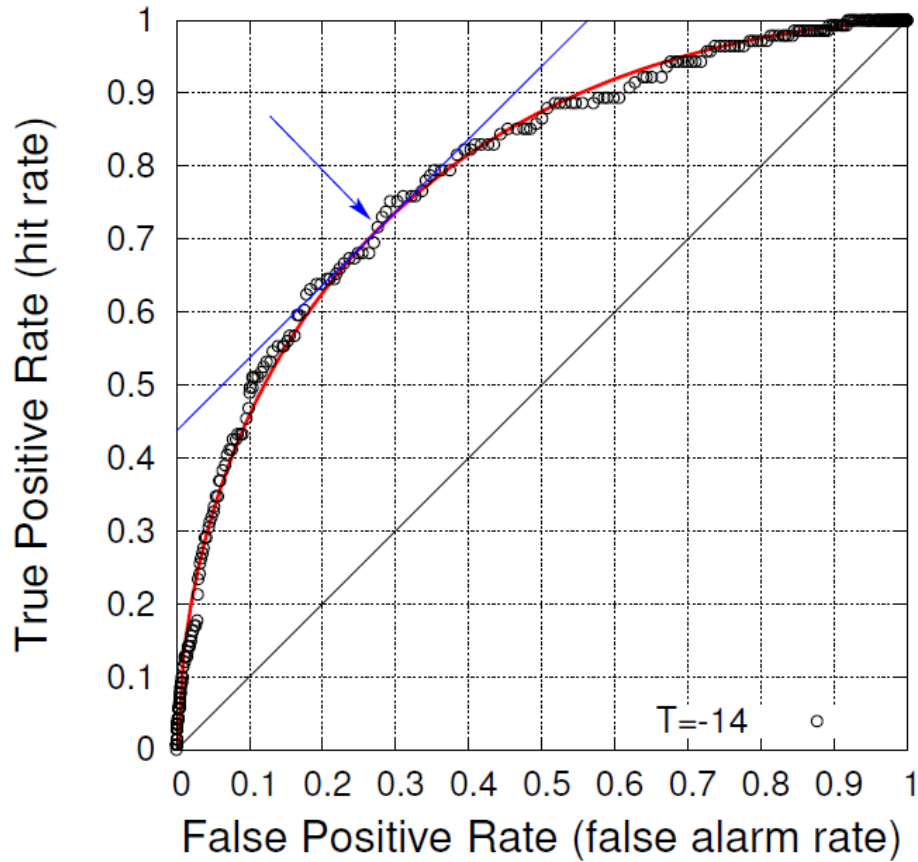
17 **Figure 4.** The PDF of ΔS_{20} (black curve, left scale) together with the corresponding histogram
18 (red bars, left scale) obtained from the time series of ΔS_{20} , which is also plotted vs. time (blue
19 crosses, right scale) along the vertical axis. The arrows indicate when ΔS_{20} exceeds 0.0205
20 and are labeled by the corresponding ongoing strong El Niño events.

21



1

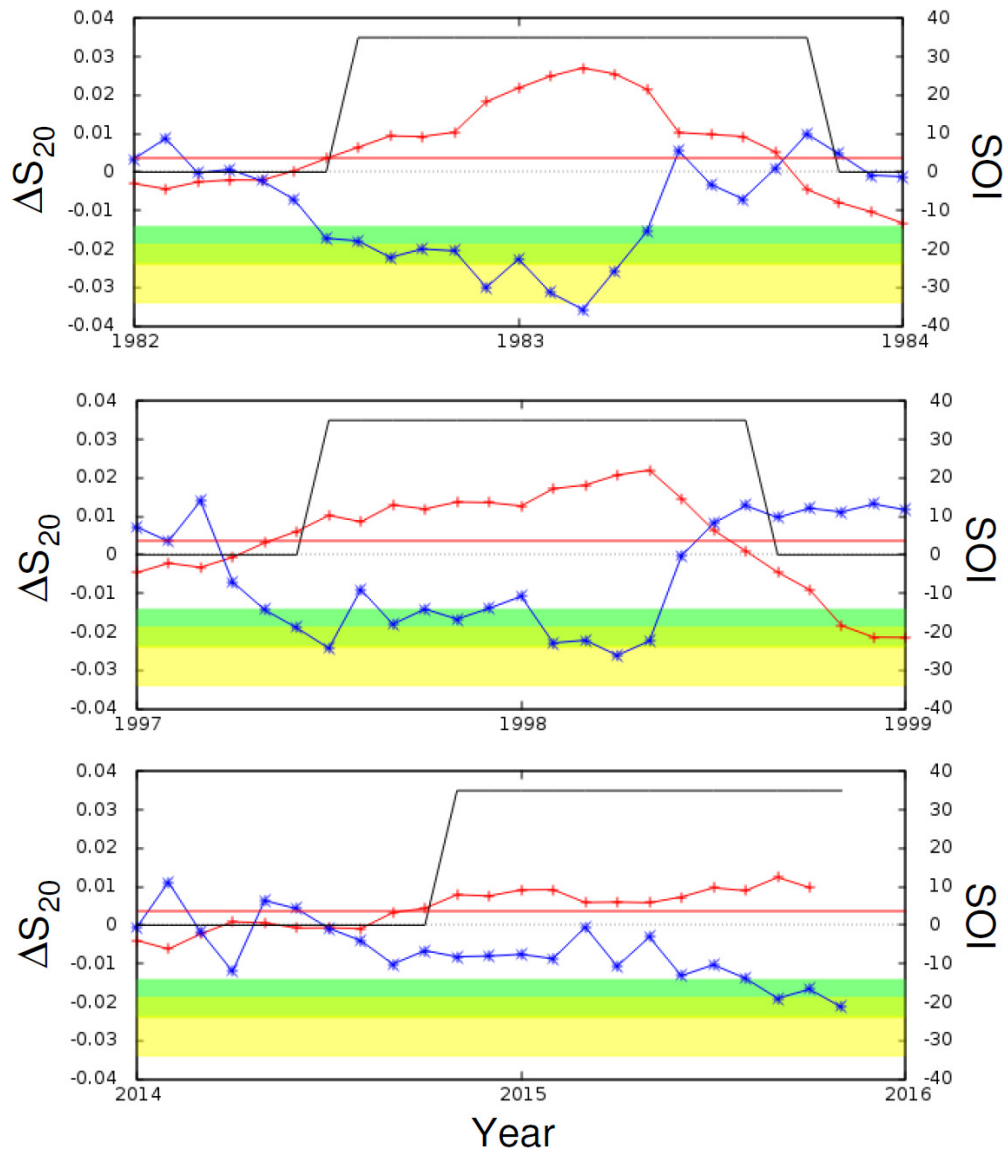
2 **Figure 1.** The entropy change ΔS_{20} in natural time for the window length $i = 20$ months (red
 3 line, left scale) along with SOI monthly values (blue line, right scale) for the period January
 4 1980 – October 2015. The alarm is set on (black line), when ΔS_{20} exceeds the threshold value
 5 $\Delta S_{\text{thres}} = 0.0035$.



1

2

3 **Figure 2.** The hit rate vs. false alarm rate when using ΔS_{20} as a predictor for the SOI value of
 4 the next month. The ROC point indicated by the arrow has been selected so that the slope of
 5 the tangent of the analytical fitting of the ROC points indicated by the red curve has unit slope
 6 and hence it corresponds to the $m = 1$ iso-performance line of the ROC space (e.g., see
 7 Fawcett, 2006; Provost and Fawcett, 1998, 2001).

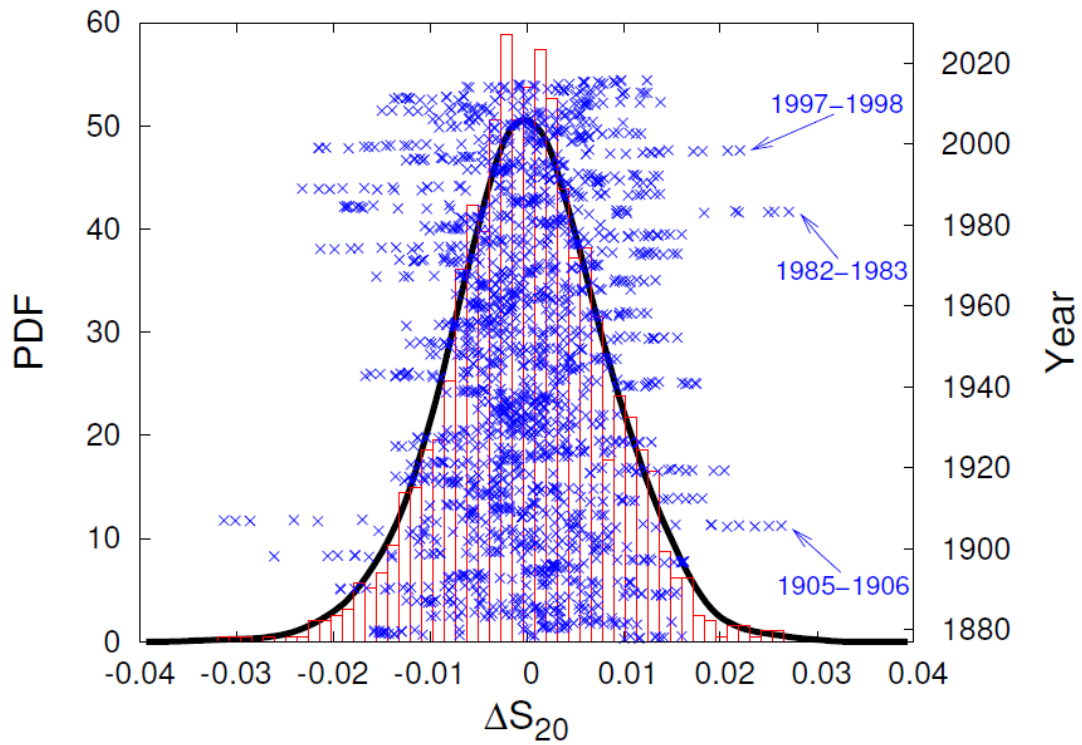


1

2

3 **Figure 3.** As in Fig. 1, but only for the 1982–1983, 1997–1998 (the two strongest in the last

4 century) and the current 2015–2016 El Niño events.



1

2

3 **Figure 4.** The PDF of ΔS_{20} (black curve, left scale) together with the corresponding histogram
 4 (red bars, left scale) obtained from the time series of ΔS_{20} , which is also plotted vs. time (blue
 5 crosses, right scale) along the vertical axis. The arrows indicate when ΔS_{20} exceeds 0.0205
 6 and are labeled by the corresponding ongoing strong El Niño events.

7